Wetting properties of thin films of exfoliated hexagonal boron nitride in different solvents

S. Acosta[a], V. Pérez-Luna[a], G. Sánchez-Balderas[b], J. M. Hernández-Meza[b], B. Yáñez-Soto[c], and M. Quintana[a,d]

[a]*Centro de Investigación en Ciencias de la Salud y Biomedicina, Universidad Autónoma de San Luis Potosí, Av. Sierra Leona 550, Lomas de San Luis, 78210, San Luis Potosí, México.*

[b]*Instituto de Física, Universidad Autónoma de San Luis Potosí, Av. Parque Chapultepec 1570, Privadas del Pedregal, 78295, San Luis Potosí, México.*

[c]*CONACyT-Instituto de Física, Universidad Autónoma de San Luis Potosí, Av. Parque Chapultepec 1570, Privadas del Pedregal, 78295, San Luis Potosí, México.*

[d] *Facultad de Ciencias, Universidad Autónoma de San Luis Potosí, Av. Parque Chapultepec 1570, Privadas del Pedregal, 78295, San Luis Potosí, México.*

Received 8 December 2022; accepted 25 January 2023

Hexagonal boron nitride is a 2D material with excellent properties, such as large band gap, high thermal and chemical stability, transparency, and high oxidation and corrosion resistance. These properties make h-BN a suitable candidate to be used in the development of advanced coatings. However, as for other nanomaterials, tailoring and controlling the properties of h-BN is a fundamental key to its application into several fields. Here, the wetting properties of h-BN were investigated when it is exfoliated by ultrasonic cavitation in different solvents such as isopropyl alcohol (IPA), dioxane (Dx), N-methyl pyrrolidone (NMP) and dimethyl formamide (DMF). The wetting properties of the different h-BN materials were determined by measuring the water contact angle (WCA) of h-BN thin films deposited on silicon dioxide. Different contact angles were observed for each sample, the different WCA values are explained by the differences in the structure and roughness of the thin film surfaces obtained just by changing the solvent during exfoliation. These surface properties were characterized by optic and transmission electronic microscopy (TEM) as well as atomic force microscopy (AFM).

Keywords: Hexagonal boron nitride; wettability; roughness; liquid-phase exfoliation.

DOI: https://doi.org/10.31349/RevMexFis.69.041607

1. Introduction

2D materials are important objects of study due to their remarkable and exceptional properties, compared with their bulk counterparts. Most of these 2D materials are obtained from highly ordered crystalline solids and can be classified by their chemical nature and structure as: hexagonal nanosheets, like graphene and boron nitride, transition metal oxides (TMOs) such as MnO_2, transition metal carbides or MXenes like $Ti_3C_2T_x$, and transition metal dichalcogenides (TMDs) such as MoS_2 [1–3]. Among these materials, hexagonal boron nitride (h-BN) is a 2D layered material, each layer conformed of boron (B) and nitrogen (N) atoms in equal atomic concentration, which are covalently bonded trough a sp^2-hybridized configuration with a bond length of 1.44 Å [4], a structure similar to graphene. The layers interact among each other by van der Waals forces and, due to the polarity of the B-N bond, the stacking of the layers occurs with a B atom located just above or below a N atom in the neighboring sheet with an interlayer spacing of 0.33 nm [5, 6].

h-BN has a direct band gap of 6 eV whereby is an insulator and transparent material [7]. It also has an efficient light emission in the deep ultraviolet and ultraviolet regions which makes it a suitable material to be used in deep UV optoelectronic devices [8–11]. Moreover, h-BN has a high thermal stability, a monolayer of h-BN is stable up to 800°C in air compared to graphene that oxidizes at 300°C [12, 13]. Besides, this material shows a thermal conductivity of 100-270 $W\,m^{-1}K^{-1}$ h-BN [14,15], chemical inertness and a high oxidation and corrosion resistance. These make h-BN an important prospect material for developing protection coatings of metals and air-sensitive materials with applications involving high temperatures processes [16–18]. Furthermore, the insulating character of h-BN may allow the development of coatings that inhibit galvanic corrosion preventing the degradation and deterioration of the active materials in electrical and optical devices [5, 17]. Due to these remarkable properties, h-BN has also potential to be used as dielectric substrate for other materials, such as graphene and MoS_2 [19, 20].

Regarding to the mechanical properties, h-BN has a Young's modulus of 0.85 TPa and a fracture strength of 70 GPa which does not depend of the number of layers, remaining constant up to 9 layers, as observed by Aleksey and collaborators [21], contrary to graphene, whose strength decreases considerably with the number of layers. These properties make h-BN the strongest insulator material with promising applications on mechanical reinforcement [21].

The wettability is a surface property related to the interaction of liquid molecules with the atoms at the surface of a material [22, 23]. Therefore, this property depends on the ordered structure of the surface, the surface roughness [24], the surface chemistry, and the surface energy [25, 26]. The wet-

tability is determined by measuring the contact angle (CA) of the surface material, in the case of water, it is commonly called water contact angle (WCA). Tailoring and controling this property in nanomaterials, especially for 2D materials, is an important key to its their application in many fields, such as the development of coatings for anti-corrosion and anti-biofouling, self-healing, energy generation and medical applications [25, 27–29]. For the case of h-BN, the theory predicts values for WCA of 86°, as reported by Li Hui and Xiao Zeng [30]. However, when the WCA was experimentally measured by Lee and collaborators, the measured WCA was 50° [31]. This difference was explained by the defects created in h-BN during the synthesis method, which proves that the synthesis and processing methods of nanomaterials have a great influence in their final structure and properties. 2D h-BN, like other 2D materials, has been produced mainly by mechanical exfoliation, liquid-phase exfoliation, and chemical vapor deposition (CVD) [5, 32, 33]. Performing mechanical exfoliation allows the production of high-quality h-BN, but at low yield and with randomly distributed layers [34]. CVD methods allow to control the number of layers and, in a limited way, the size of the sheets. Nevertheless, a high reaction temperature is required and often the transfer of the synthetized material onto different substrates is complicated and induce defects in the layered material which can lead to a non-controlled variation on the properties of h-BN [35, 36]. Although liquid-phase exfoliation has the drawbacks of small sheets sizes production and surface contamination from the solvents used, it is still considered an efficient method to produce good quality h-BN in a low-cost manner and high yield concentration [37]. Liquid-phase exfoliation of h-BN was first reported by Han and collaborators in 2008 [38]. The solvent used during exfoliation plays a fundamental role in the production of 2D materials. To accomplishes the exfoliation of the layers, the surface tension of the solvent must match the energy of the 2D material so it can overcome the van der Waals forces among the layers and minimize the energy of exfoliation leading to a good dispersion of the exfoliated layers. As it has been exhaustively demonstrated, the synthesis method has an important effect in the properties of the obtained material [39, 40]. This aspect can be used as an advantage for tailoring and controlling certain properties of the materials by changing the synthesis method and its parameters. Here, the wetting properties of h-BN were evaluated when this material was obtained by liquid-phase exfoliation using different solvents (isopropyl alcohol (IPA), dioxane (Dx), N-methyl pyrrolidone (NMP) and N,N-dimethylformamide (DMF)) and deposited as a thin film in silicon dioxide (SiO_2), demonstrating that the solvent used during exfoliation has a direct effect in the wetting properties of the film, and that in this way, films with specific wetting properties for different applications can be obtained.

2. Methods

2.1. Materials and reagents

Boron nitride powder ($\sim$ 1μm, 98%) was purchased from Sigma-Aldrich, chemicals, and solvents, isopropyl alcohol (IPA), dioxane (Dx), N-methyl pyrrolidone (NMP) and dimethyl formamide (DMF) were used without further purification.

2.2. Methodology

2.2.1. Liquid-phase exfoliation of boron nitride

Hexagonal boron nitride (h-BN) was produced by sonication, using a sonic bath Branson 2510. Samples were prepared by the exfoliation of h-BN in different solvents: a. Isopropyl alcohol (IPA), b. p-Dioxane (Dx), c. N,N-Dimethylformamide (DMF) and d. N-Methyl-2-pyrrolidone (NMP). All samples were sonicated for 3 h. After sonication, the samples were centrifuged at 2000 rpm for one hour and the precipitated was removed. Finally, the resulting materials were washed and dispersed in their corresponding fresh solvent.

2.3. Characterization techniques

Absorption measurements were carried out by UV-Vis spectroscopy with an Agilent Cary 60. The concentration of h-BN in IPA, Dx, NMP and DMF was determined by absorption spectroscopy. Initial concentration for all the samples was 3 mg/mL. The absorbance of the filtered samples was measured every three days for a 30-day period, not significant change was observed.

Static water contact angles (WCAs) were measured using a Ramé-Hart NRL C.A. goniometer, model 295-U1. Samples were prepared by drop casting the h-BN dispersions (at a 3 mg/mL concentration) onto a silicon dioxide surface which was cleaned and dried prior to the deposition. The produced films were dried under vacuum for 24 hr. The WCAs were measured on 5 μL water droplets at four different locations on each sample. All measurements were done at room temperature and the WCA was measured four times for each sample, the reported WCA is the mean of these values.

Roughness measurements were carried out by using an Atomic Force Microscopy (AFM) Dimension Edge Bruker Instrument. AFM images were obtained using tapping mode at RT, with a silicon tip (Model: OTESPA-R3), scanning rate of 40 μm/s (0.2 Hz), image resolution of 512×512 and scan X-Y range of 50 μm and 100 μm. Image analysis was performed using NanoScope Analysis 1.4.

Transmission electron microscopy (TEM) images were acquired using a TEM JEOL JEM-2100, and an accelerating voltage of 200 kV. Samples were prepared by drop casting of stable dispersions onto a TEM grid (200 mesh, Lacey carbon films). Optical images of the h-BN films were obtained with an Olympus BX41 optical microscope.

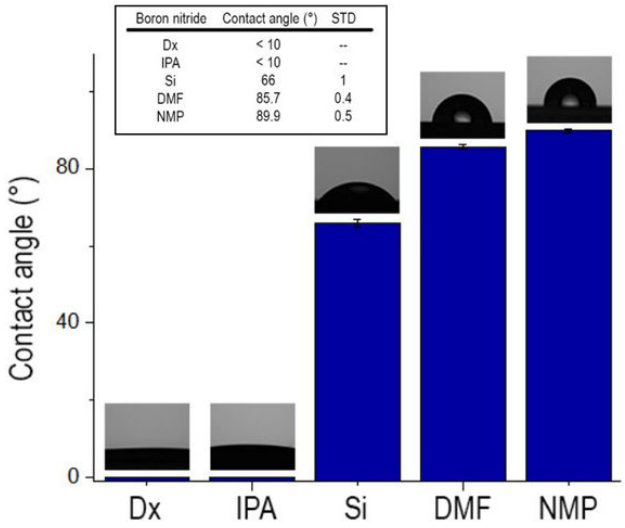

FIGURE 1. Average water contact angle values (WCAs) for exfoliated h-BN in different solvents and deposited on silicon oxide surface.

TABLE I. Parameters obtained from the UV-vis absorption characterization of all h-BN exfoliated samples.

Solvent	λ (nm)	A (Arb. units)	α (L/mon cm)	Final concentration (mol/L)
Dx	228	1.27	466	0.11
IPA	274	0.27	586	0.12
DMF	322	0.30	240	0.10
NMP	276	0.33	306	0.10

3. Results and discussion

First, h-BN was obtained by liquid-phase exfoliation in different solvents: a) p-Dioxane (Dx), b) Isopropyl alcohol (IPA), c) N,N-Dimethylformamide (DMF) and d) N-Methyl-2-pyrrolidone (NMP). It is important to note that all the used solvents own a polar character except for p-Dioxane. The final concentration after the sonication process was determined by UV-vis absorption spectroscopy. Absorbance versus concentration was plotted for h-BN in Dx, IPA, DMF and NMP to obtain the values for the absorption coefficient (α) for each sample. All measurements showed Lambert-Beer behavior, allowing the calculation of α values: $\langle\alpha_{228}\rangle = 466$ L/mol cm (Dx-hBN), $\langle\alpha_{228}\rangle = 586$ L/mol cm (IPA-hBN), $\langle\alpha_{228}\rangle = 240$ L/mol cm (DMF-hBN) and $\langle\alpha_{228}\rangle = 306$ L/mol cm (NMP-hBN) (Table I). The highest concentration yield was observed for isopropanol (IPA-hBN) (Table I), as reported by Coleman and collaborators who observed that exfoliation of h-BN using IPA as solvent leads to an almost 50% of dispersions yield [41].

The WCAs measurements of the produced thin films of h-BN are shown in Fig. 1, the h-BN thin films yield different values depending on the solvent used during the exfoliation of the sample. NMP-hBN film yields a contact angle of 89.9°, DMF-hBN film 85.7° in good agreement with the theoretical WCAs value [31], while the WCA of Dx-hBN and IPA-hBN films were not measurable because of their low value. From these values it is clear to observe that effectively the selection of the solvent during the exfoliation has an effect in the wetting properties of the obtained h-BN film. To elucidate this effect, the samples were analyzed by optical and transmission electronic microscopy (TEM) as well as atomic force microscopy (AFM) to determine the surface structure and surface roughness of the samples.

Figure 2 shows the TEM microscopy of the h-BN samples. In all the samples is observed the obtention of small

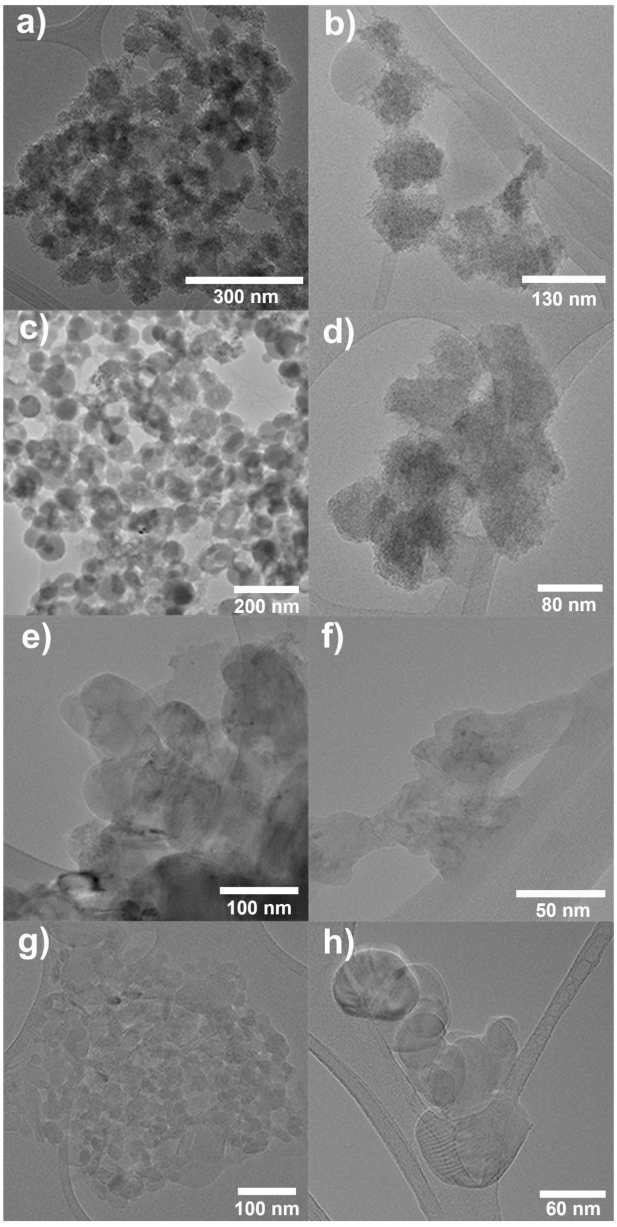

FIGURE 2. TEM images of h-BN exfoliated in: a)-b) p-Dioxane, c)-d) Isopropyl Alcohol, e)-f) DMF, g)-h) NMP.

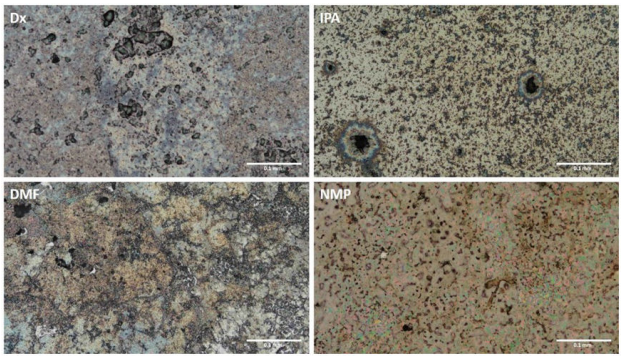

FIGURE 3. Optical images on large-scale views of the h-BN samples.

lateral sized h-BN sheets, this is attributed to the long period of time of sonication and the cavitation phenomenon that contributes to cutting of the lateral dimensions of the h-BN sheets. All samples showed similar lateral size, the materials are observed as few layer crystals mixed with exfoliated nanosheets. For the case of h-BN exfoliated in DMF (Figs. 2e)-f)) and NMP (Figs. 2g)-h)) smoothest surfaces are observed, while in NMP exfoliated nanosheets were more frequently observed. NMP is the solvent with the highest surface tension compared with the other solvents. The surface tension of isopropyl alcohol is 23.0 mN/m^2, for dioxane is 33.0 mN/m^2, for DMF is 37.1 mN/m^2 and for NMP is 40.79 mN/m^2.

Optical photographs of the h-BN films produced were taken for a large-scale view of the samples and are shown in Fig. 3. The films prepared from dispersion of h-BN in IPA and NMP are more homogeneous than films prepared by the deposition of h-BN dispersed in Dx and DMF which are observed as a heterogeneous distribution of h-BN clusters. This better homogeneity could be related to the creation of more stable dispersion and a lower agglomeration of h-BN layer crystals in the solvents IPA and NMP.

The surface roughness of the h-BN thin films was measured using tapping mode AFM. Topological and three-dimensional AFM images of the samples are shown in Fig. 4, the height histograms for each sample are shown graphically in Fig. 5 and the root-mean-square (rms) roughness values are shown in Table II. In the topology and 3D AFM images of the Dx-hBN sample (Fig. 4a)-b)) the presence of peaks of different sizes is observed, with heights that vary from 2 to 3 μm (Fig. 5). This heterogeneity of the surface was also observed in the large-scale view image and explains the presence of the largest rms roughness of 0.32 μm compared with the other samples (Table II). On the other hand, the IPA-hBN film has a homogeneous surface with well distributed small clusters of h-BN particles (Fig. 4c)) which could be responsible for its low rms roughness of 0.09 μm, being the film with the lowest value of all the samples.

In addition, the IPA-hBN film has the lowest and most uniform height distribution [Figs. 5 and Fig. 4d)]. Large clusters are also observed in this film (Fig. 3 IPA), which were not scanned by AFM due to their size. These large clusters

TABLE II. RMS roughness (Rrms), average roughness (Ra) and maximum roughness depth (Rmax) of h-BN samples (100 micrometers).

Hexagonal Boron Nitride	$R_{\rm rms}$ (μm)	R_a (μm)	$R_{\rm max}$ (μm)
Dx	0.32 ± 0.07	0.22 ± 0.07	3.35 ± 0.51
IPA	0.09 ± 0.04	0.06 ± 0.02	1.54 ± 0.64
DMF	0.16 ± 0.08	0.11 ± 0.05	1.63 ± 0.31
NMP	0.26 ± 0.06	0.19 ± 0.04	2.31 ± 0.70

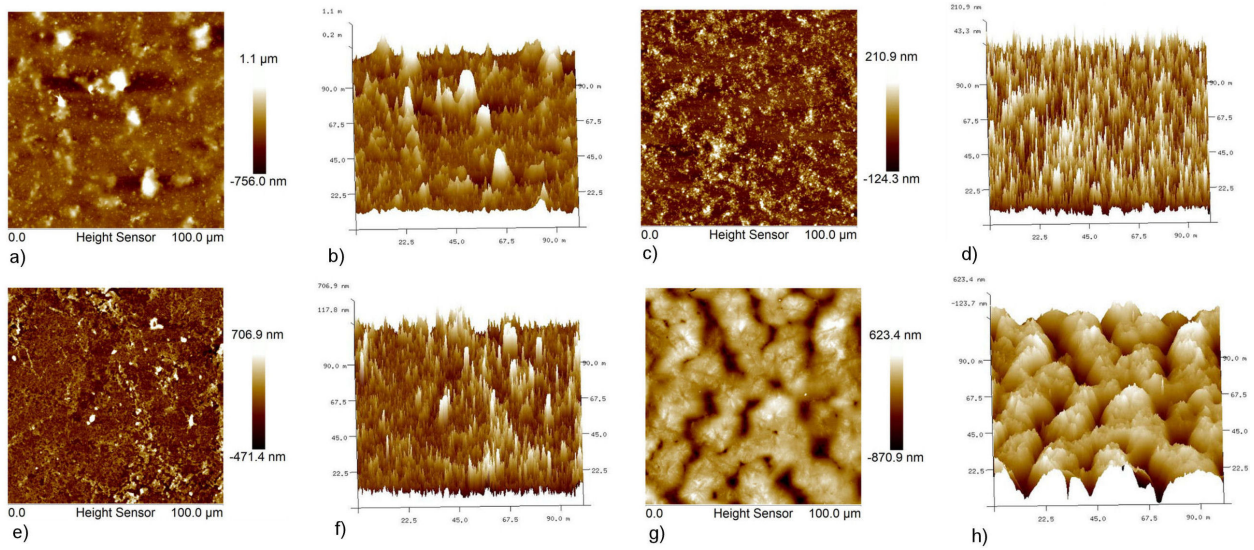

FIGURE 4. Tapping mode AFM imaging of h-BN films. Representative AFM topography and 3-dimensional images of top area of Dx-hBN a)-b), IPA-hBN (c-d), DMF-hBN e)-f) and NMP-hBN g)-h) films.

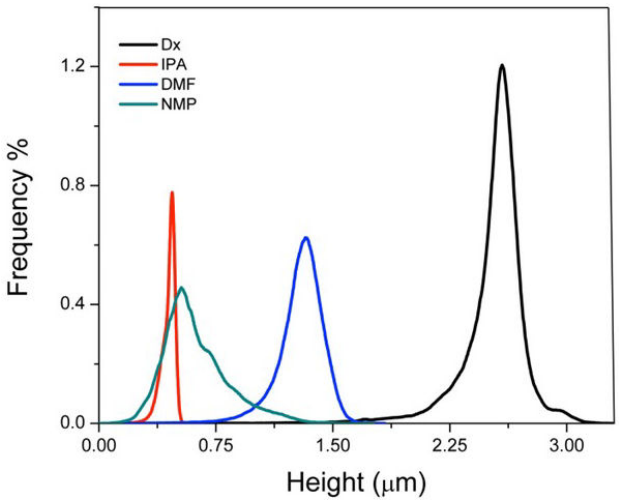

FIGURE 5. Histogram distribution of heights on the h-BN films.

may be responsible for the low WCA value. The DMF-hBN film exhibits a surface structure composed of small pronounced "crusts" with high roughness that are mixed with areas of low roughness (Figs. 4e)-f)). These "crusts" are composed by small spheres with a diameter of 150 nm, the film has a rms roughness of 0.16 μm and distribution of heights that goes from 0.75 to 1.5 μm. Finally, the NMP-hBN film has rms roughness of 0.26 μm and a morphology like a "plateau" with small peaks on it (Figs. 4g)-h)) with heights from 0.1 to 1.1 μm and a second mode in its distribution due to the contribution of the pores present in the film (Fig. 5). This homogeneous porous "netting" topology was also observed in the large-scale view image (Fig. 3 NMP) and is probably responsible for the almost hydrophobic property of the NMP-hBN film. From these results it can be observed that different surface roughness and morphologies can be generated in thin films of h-BN by modifying the solvent used during liquid-phase exfoliation and that these changes in the roughness have influence in the wetting properties of the films. Here, we observed that for the case of IPA-hBN, DFM-hBN and NMP-hBN thin films, an increase in the rms roughness of the films leads to an increased WCA value as reported by Miller and collaborators [42]. However, this was not observed for the Dx-hBN film which has the highest rms roughness but WCA less than 10°. This anomaly can be related to several phenomena. The nonpolar character of p-dioxane may lead to a low dissolution of the h-BN layers, which causes the creation of large h-BN aggregates that then make non-possible to measure the water contact angle. However, this low WCA can be also related to the wetting anisotropy effect that is explained by the creation of heterogeneous patterns or nanostructures on the surface of the films that leads to discontinuities were unsaturated atoms at the edges of the sheets or crystallites can be functionalized with terminations like -OH and -H groups. These terminal bonds cause a change in the interaction with water molecules, even though there is no functionalization of the edges, they will also have an effect in the interaction of the film with the liquid. This changes in the interaction of the film with water molecules can lead to an effective anisotropy of the wetting properties resulting in an increase or decrease of the WCA [43–45].

4. Conclusions

By changing the solvent used during liquid-phase exfoliation of h-BN the wetting properties of h-BN thin films can be modified. The use of different solvents leads to a production of films with different morphologies and roughness surfaces, which in turn leads to a change in the water contact angle of the films. Here, we observed that an increase on the rms roughness leads to an increased WCA, with exception of an h-BN thin film prepared from h-BN dispersed in dioxane, whose high roughness can lead to an anisotropy wettability. These results show that the properties of nanostructured materials depend critically on the synthesis methods and its parameters, and that in this way, we are able of control and tailor certain properties, such as wettability, to produce surfaces with precise properties for specific applications. The differences in WCA of exfoliated h-BN might allow the ease integration into a matrix with different polarities at relatively large concentrations.

1. L. Niu, *et al*., Production of two-dimensional nanomaterials via liquid-based direct exfoliation, *Small* **12** (2016) 272. https://doi.org/10.1002/smll.201502207.

2. S. Z. Butler, *et al*., Progress, challenges, and opportunities in two-dimensional materials beyond graphene, *ACS nano* **7** (2013) 2898. https://doi.org/10.1021/nn400280c.

3. R. Ma and T. Sasaki, Two-dimensional oxide and hydroxide nanosheets: controllable high-quality exfoliation, molecular assembly, and exploration of functionality, *Accounts of chemical research* **48** (2015) 136. https://doi.org/10.1021/ar500311w.

4. L. H. Li, *et al*., Large-scale mechanical peeling of boron nitride nanosheets by low-energy ball milling, *Journal of materials chemistry* **21** (2011) 11862. https://doi.org/10.1039/C1JM11192B.

5. K. Zhang, *et al*., Two dimensional hexagonal boron nitride (2DhBN): synthesis, properties and applications, *Journal of Materials Chemistry C* **5** (2017) 11992. https://doi.org/10.1039/C7TC04300G.

6. Q. Weng, *et al*., Functionalized hexagonal boron nitride nanomaterials: emerging properties and applications, *Chemical Society Reviews* **45** (2016) 3989. https://doi.org/10.1039/C5CS00869G.

7. K. Watanabe, T. Taniguchi, and H. Kanda, Direct-bandgap properties and evidence for ultraviolet lasing of hexagonal boron nitride single crystal, *Nature materials* **3** (2004) 404. https://doi.org/10.1038/nmat1134.
8. L. Hua Li, *et al*., Photoluminescence of boron nitride nanosheets exfoliated by ball milling, *Applied Physics Letters* **100** (2012) 261108. https://doi.org/10.1063/1.4731203.
9. L. Li, *et al*., High-quality boron nitride nanoribbons: unzipping during nanotube synthesis, *Angewandte Chemie* **125** (2013) 4306. https://doi.org/10.1002/ange.201209597.
10. L. Schué, *et al*., Dimensionality effects on the luminescence properties of hBN, *Nanoscale* **8** (2016) 6986. https://doi.org/10.1039/C6NR01253A.
11. R. Bourrellier, *et al*., Bright UV single photon emission at point defects in h-BN, *Nano letters* **16** (2016) 4317. https://doi.org/10.1021/acs.nanolett.6b01368.
12. L. H. Li, *et al*., Strong oxidation resistance of atomically thin boron nitride nanosheets, *ACS nano* **8** (2014) 1457. https://doi.org/10.1021/nn500059s.
13. L. Liu, *et al*., Graphene oxidation: thickness-dependent etching and strong chemical doping, *Nano letters* **8** (2008) 1965. https://doi.org/10.1021/nl0808684.
14. I. Jo, *et al*., Thermal conductivity and phonon transport in suspended few-layer hexagonal boron nitride, *Nano letters* **13** (2013) 550. https://doi.org/10.1021/nl304060g.
15. M. Alam, *et al*., Thermal conductivity of ultra-thin chemical vapor deposited hexagonal boron nitride films, *Applied Physics Letters* **104** (2014) 013113. https://doi.org/10.1063/1.4861468.
16. L. H. Li and Y. Chen, Atomically thin boron nitride: unique properties and applications, *Advanced Functional Materials* **26** (2016) 2594. https://doi.org/10.1002/adfm.201504606.
17. L. H. Li, *et al*., Boron nitride nanosheets for metal protection, *Advanced materials interfaces* **1** (2014) 1300132. https://doi.org/10.1002/admi.201300132.
18. X. Li, *et al*., Large area hexagonal boron nitride monolayer as efficient atomically thick insulating coating against friction and oxidation, *Nanotechnology* **25** (2014) 105701. https://doi.org/10.1088/0957-4484/25/10/105701.
19. C. R. Dean, *et al*., Boron nitride substrates for high-quality graphene electronics, N*ature nanotechnology* **5** (2010) 722. https://doi.org/10.1038/nnano.2010.172.
20. L. Britnell, *et al*., Field-effect tunneling transistor based on vertical graphene heterostructures, *Science* **335** (2012) 947. https://doi.org/10.1126/science.1218461.
21. A. Falin, *et al*., Mechanical properties of atomically thin boron nitride and the role of interlayer interactions, *Nature communications* **8** (2017) 15815. https://doi.org/10.1038/ncomms15815.
22. X. Li, *et al*., Wettability of supported monolayer hexagonal boron nitride in air, *Advanced functional materials* **27** (2017) 1603181. https://doi.org/10.1002/adfm.201603181.
23. I. Mata-Cruz, *et al*., Mimicking rose petal wettability by chemical modification of graphene films, *Carbon* **121** (2017) 472. https://doi.org/10.1016/j.carbon.2017.06.018.
24. G. Sánchez-Balderas and E. Pérez, On the usefulness of the equation of state approach for contact angles on rough surfaces, *Applied Physics A* **126** (2020) 20. https://doi.org/10.1007/s00339-019-3177-5.
25. A. Kumar, *et al*., Controllable synthesis of tunable aspect ratios novel h-BN nanorods with an enhanced wetting performance for water repellent applications, *Vacuum* **184** (2021) 109927. https://doi.org/10.1016/j.vacuum.2020.109927.
26. G. Sánchez-Balderas, J. H. Velázquez, and E. Pérez, Dependence of the Liquid Polarity in the Wetting of Rough Surface: An Effective Surface Tension Approach, *Langmuir* **38** (2022) 12804. https://doi.org/10.1021/acs.langmuir.2c01582.
27. K. Kubiak, *et al*., Wettability versus roughness of engineering surfaces, *Wear* **271** (2011) 523. https://doi.org/10.1016/j.wear.2010.03.029.
28. F. Mahvash, *et al*., Corrosion resistance of monolayer hexagonal boron nitride on copper, *Scientific reports* **7** (2017) 42139. https://doi.org/10.1038/srep42139.
29. L. B. Boinovich, *et al*., Origins of thermodynamically stable superhydrophobicity of boron nitride nanotubes coatings, *Langmuir* **28** (2012) 1206. https://doi.org/10.1021/la204429z.
30. H. Li and X. C. Zeng, Wetting and interfacial properties of water nanodroplets in contact with graphene and monolayer boron-nitride sheets, *ACS nano* **6** (2012) 2401. https://doi.org/10.1021/nn204661d.
31. C. H. Lee, J. Drelich, and Y. K. Yap, Superhydrophobicity of boron nitride nanotubes grown on silicon substrates, *Langmuir* **25** (2009) 4853. https://doi.org/10.1021/la900511z.
32. M. Velick'y, *et al*., Exfoliation of natural van der Waals heterostructures to a single unit cell thickness, *Nature Communications* **8** (2017) 14410. https://doi.org/10.1038/ncomms14410.
33. H. Liu, *et al*., Synthesis of hexagonal boron nitrides by chemical vapor deposition and their use as single photon emitters, *Nano Materials Science* **3** (2021) 291, https://doi.org/10.1016/j.nanoms.2021.03.002.
34. D. Pacile, *et al*., The two-dimensional phase of boron nitride: Few-atomic-layer sheets and suspended membranes, *Applied Physics Letters* **92** (2008) 133107, https://doi.org/10.1063/1.2903702.
35. J.-H. Park, *et al*., Thickness-controlled multilayer hexagonal boron nitride film prepared by plasma-enhanced chemical vapor deposition, *Current Applied Physics* **16** (2016) 1229, https://doi.org/10.1016/j.cap.2016.03.025.
36. A.-R. Jang, *et al*., Wafer-scale and wrinkle-free epitaxial growth of single-orientated multilayer hexagonal boron nitride on sapphire, *Nano letters* **16** (2016) 3360, https://doi.org/10.1021/acs.nanolett.6b01051.

37. C. Zhi, *et al*., Large-scale fabrication of boron nitride nanosheets and their utilization in polymeric composites with improved thermal and mechanical properties, *Advanced materials* **21** (2009) 2889, https://doi.org/10.1002/adma.200900323.

38. W.-Q. Han, *et al*., Structure of chemically derived mono-and few-atomic-layer boron nitride sheets, *Applied Physics Letters* **93** (2008) 223103, https://doi.org/10.1063/1.3041639.

39. G. Ciampalini, *et al*., Light emission properties of mechanical exfoliation induced extended defects in hexagonal boron nitride flakes, *2D Materials* **9** (2022) 035018, https://doi.org/10.1088/2053-1583/ac6f09.

40. A. J. Watson, *et al*., Transfer of large-scale two-dimensional semiconductors: challenges and developments, *2D Materials* **8** (2021) 032001. https://doi.org/10.1088/2053-1583/abf234.

41. J. N. Coleman, *et al*., Two-dimensional nanosheets produced by liquid exfoliation of layered materials, *Science* **331** (2011) 568. https://doi.org/10.1126/science.1194975.

42. J. D. Miller, *et al*., Effect of roughness as determined by atomic force microscopy on the wetting properties of PTFE thin films, *Polymer Engineering & Science* **36** (1996) 1849, https://doi.org/10.1002/pen.10580.

43. S. Gao, W. Liu, and Z. Liu, Tuning nanostructured surfaces with hybrid wettability areas to enhance condensation, *Nanoscale* **11** (2019) 459, https://doi.org/10.1039/C8NR05772A.

44. E. Wagemann, *et al*., Wettability of nanostructured hexagonal boron nitride surfaces: molecular dynamics insights on the effect of wetting anisotropy, *Physical Chemistry Chemical Physics* **22** (2020) 2488, https://doi.org/10.1039/C9CP06708F.

45. J. E. Andrews, *et al*., Roughness-induced chemical heterogeneity leads to large hydrophobicity in wetting-translucent nanostructures, *The Journal of Physical Chemistry C* **121** (2017) 10010. https://doi.org/10.1021/acs.jpcc.7b02222.